

## Appendix A1. Incorporating CO<sub>2</sub> diffusion and assimilation in OnGuard3

Models of photosynthesis often distinguish between the conductance through the stomatal pore, the conductance of gaseous diffusion within the leaf, and the conductance of the mesophyll cell<sup>1</sup>. The primary barrier to diffusion is generally recognized to occur at the stoma, with a second barrier occurring as CO<sub>2</sub> dissolves and passes through the aqueous and lipid phases of the mesophyll cell to enter the chloroplast<sup>1-3</sup>. Thus, it is to be expected that there is less variation in the partial pressure of CO<sub>2</sub> within the intercellular air space, and this interpretation accords with estimates of diffusion of CO<sub>2</sub> within leaves<sup>4-6</sup>. For the guard cell, the primary variable of interest is the partial pressure of CO<sub>2</sub> in the substomatal cavity,  $pC_i$ , with which the guard cells equilibrate. Thus, we subsume the conductances of gaseous diffusion within the leaf and the mesophyll and assign  $pC_i$  to  $p$  that represents all points midway in fractional resistance along the diffusion pathway from the atmosphere to the mesophyll. We resolve  $pC_i$ , assuming that CO<sub>2</sub> consumed by carbon assimilation,  $-a$ , in the mesophyll under each stoma of the leaf will be replaced by CO<sub>2</sub> entering through the stomatal pore in the steady state (Figure 1).

From Fick's Law the rate of flux of CO<sub>2</sub> through the stoma

$$j_s = A_s D_c (pCO_2 - pC_i) / d_s = -a \quad [A1]$$

where  $A_s$  is the cross-sectional area of the stoma,  $D_c$  is the CO<sub>2</sub> diffusion coefficient in air,  $d_s$  is the depth of the stomatal pore, and  $pCO_2$  and  $pC_i$  are the partial pressures of CO<sub>2</sub> in the atmosphere and at  $p$  in the substomatal cavity, respectively (a complete list of parameters is included in Supplemental Table 1). Rearranging Equation [A1] gives

$$pC_i = pCO_2 - a d_s / A_s D_c \quad [A2]$$

after adjusting the rate of assimilation for its absolute value. The rate of carbon assimilation under each stoma,  $a$ , in turn depends on both fluence rate of photosynthetically-active radiation,  $I$ , and on CO<sub>2</sub> within the mesophyll<sup>1,7,8</sup>. Thus, for the mesophyll under each stoma, the dependence of assimilation on light can be approximated as

$$a = a_L a_C - r_d \quad , \quad [A3a]$$

$$a_L = (\phi I + a_{max} - [(\phi I + a_{max})^2 - 4\Theta\phi a_{max} I]^{0.5}) / 2\Theta \quad , \text{ and} \quad [A3b]$$

$$a_C = 1 / [1 + K_C / (pC_i - C_c)] \quad [A3c]$$

where  $a_L$  and  $a_C$  describe the light- and CO<sub>2</sub>-limited components of carbon assimilation,  $r_d$  is the respiration rate in the dark,  $\phi$  is the quantum efficiency of assimilation,  $a_{max}$  is the

maximum rate of assimilation at saturating partial pressures of CO<sub>2</sub>, and  $\Theta$  is a dimensionless constant defining the non-rectangular transition between light- and RubisCO-limited characteristics of assimilation. At saturating light intensities,  $K_C$  defines the  $K_{1/2}$  for CO<sub>2</sub> fixation and  $C_C$  is the photorespiratory CO<sub>2</sub> compensation point.

We assume that  $pC_i$  equilibrates with dissolved CO<sub>2</sub> in accord with its solubility constant  $K_{CO_2}$  such that

$$[CO_2]_{aq} = [H_2CO_3] = pC_i K_{CO_2} \quad . \quad [A4]$$

This equilibration is assumed to go to completion within each iteration of OnGuard3, consistent with the high turnover rates of carbonic anhydrases<sup>9,10</sup>.

Dissolved CO<sub>2</sub> is the substrate for RuBisCO-mediated assimilation, but it will also equilibrate with the dissociated carbonate species such that the fractional amounts,  $\alpha$ , of each species is defined at a given pH by

$$\alpha_{H_2CO_3} = [H^+]^2 / ([H^+]^2 + [H^+]K_{a1} + K_{a1}K_{a2}) \quad , \quad [A5a]$$

$$\alpha_{HCO_3^-} = [H^+]K_{a1} / ([H^+]^2 + [H^+]K_{a1} + K_{a1}K_{a2}) \quad , \text{ and} \quad [A5b]$$

$$\alpha_{CO_3^{2-}} = K_{a1}K_{a2} / ([H^+]^2 + [H^+]K_{a1} + K_{a1}K_{a2}) \quad , \quad [A5c]$$

where  $K_{a1}$  and  $K_{a2}$  are the dissociation constants for H<sub>2</sub>CO<sub>3</sub> and HCO<sub>3</sub><sup>-</sup>, respectively. These relations are important, because HCO<sub>3</sub><sup>-</sup> is the ligand proposed to regulate membrane transport in the guard cell.

Finally, to scale models from the single stoma to the whole leaf and determine the CO<sub>2</sub> flux associated with  $g_s$ , we assign each stoma the underlying fraction of the total intercellular air space of the leaf for gas exchange and the complementary fraction of mesophyll cells, as before<sup>11</sup>. Thus, the intercellular volume,  $V_S$ , and mesophyll volume,  $V_M$ , assigned to each stoma

$$V_S = d_e V_F / D_S \quad \text{and} \quad V_M = 1 - V_S \quad [A6a,b]$$

serve as scalars where the values,  $d_e$  and  $V_F$  are the depth of the mesophyll cell layer and the volume fraction that is air space within the leaf, respectively, and  $D_S$  is the stomatal density over the leaf surface. In turn, the CO<sub>2</sub> flux and assimilation scales to leaf surface as

$$J_S = j_s D_S \quad \text{and} \quad A = a D_S \quad [A7a,b]$$

where  $J_s$  and  $A$  are the  $\text{CO}_2$  flux and net assimilation per unit surface area of the leaf. The parameters in Equation [A3] may similarly be scaled so that  $a_L$  gives  $A_L$ ,  $r_d$  gives  $R_d$ , and so on.

**Supplemental Table 1. OnGuard3 parameters and constants.**

---

Abbreviation	Definition
$A$	Carbon assimilation rate
$a$	Carbon assimilation rate (per stoma)
$a_L$	Light-dependent carbon assimilation rate per stoma at saturating $\text{CO}_2$
$a_C$	Factor adjusting carbon assimilation rate for $\text{CO}_2$ limitation
$a_{\max}$	Maximum carbon assimilation rate at saturating $\text{CO}_2$
$\alpha_{\text{H}_2\text{CO}_3}$	Fractional component of $\text{H}_2\text{CO}_3$ in solution
$\alpha_{\text{HCO}_3^-}$	Fractional component of $\text{HCO}_3^-$ in solution
$\alpha_{\text{CO}_3^{2-}}$	Fractional component of $\text{CO}_3^{2-}$ in solution
$A_S$	Stomatal pore area
$C_C$	Photorespiratory $\text{CO}_2$ compensation point
$D_S$	Stomatal density of the leaf
$D_C$	Diffusion constant for $\text{CO}_2$ in air
$d_e$	Depth of mesophyll cell layer
$d_S$	Depth of the stomatal pore
$I$	Fluence rate of photosynthetically-active radiation
$J_S$	Flux of $\text{CO}_2$ per unit leaf surface area
$j_S$	Flux of $\text{CO}_2$ per stoma
$K_{\text{ai}}$	Dissociation constant for $\text{H}_2\text{CO}_3$ in solution
$K_{\text{a2}}$	Dissociation constant for $\text{HCO}_3^-$ in solution
$K_C$	Apparent $K_{1/2}$ for $\text{CO}_2$ of photosynthesis at saturating light
$K_{\text{CO}_2}$	Solubility constant for $\text{CO}_2$ in water
$\rho$	Site of water vapor and $\text{CO}_2$ 'sensing' within the leaf air space
$r_d$	Respiration rate in the eark
$V_F$	Air volume fraction of the leaf
$V_M$	Mesophyll volume fraction of the leaf
$V_S$	Leaf volume per stoma
$\Theta$	Transition constant between light- and RubisCO-limited assimilation
$\phi$	Quantum efficiency of carbon assimilation

---

## Appendix A2. Analysis of $pC_i$ dependencies in OnGuard3

Successful models build on the core of the OnGuard platform incorporate 10 solute transporters at the plasma membrane and 11 solute transporters at the tonoplast. Aquaporins were introduced in OnGuard2 to address water flux at the plasma membrane and accommodate the physiology arising with stomatal responses to atmospheric relative humidity<sup>11</sup>. With one exception, all of the transporters and their parameters are defined experimentally. The exception,  $V_{Ca_{in}}$ , describes an inactivating, endomembrane  $Ca^{2+}$  channel for which there is unequivocal evidence in the literature<sup>12-16</sup>, but as yet no voltage clamp study providing parametric data. The characteristics of this channel are nonetheless firmly constrained within the OnGuard platform by the requirements for charge balance, mass conservation, and the accuracy of the platform in simulating the relevant dynamics in  $[Ca^{2+}]_i$  transients and related behaviors<sup>17,18</sup>. The significance of  $V_{Ca_{in}}$  and its contribution to OnGuard modelling was set out and discussed in detail previously along with all of the transporters, metabolic and buffering reactions and their parameters used by the OnGuard platform<sup>18,19</sup>.

Expanding the modelling platform to incorporate  $CO_2$  diffusion in OnGuard3 does not introduce a unique set of new parameters intrinsic to the modelling per se but adds constants associated with  $CO_2$  diffusion and its fixation by photosynthesis set out in Appendix A1. These constants are empirically defined and, hence, are independent of any efforts directed to predictive model resolution. Instead, the challenge with OnGuard3 lies in establishing  $CO_2$  responsiveness consistent with experimental data through an informed and parsimonious assignment of  $pC_i$  sensitivity to one or more solute transporters.

We assume that  $pC_i$  - either as dissolved  $CO_2$  or  $HCO_3^-$  as noted in the main text (here we will refer to  $HCO_3^-$ , as a grasp of this compound as a solute is intuitive) - acts as a ligand and its action can be described with an apparent  $K_{1/2}$  and Hill coefficient,  $h$ , for each transport process. OnGuard3, like previous implementations of the OnGuard platform, gives the user easy access to add and remove ligands and to define the associated  $K_{1/2}$  and  $h$  parameters for ligand action. Thus, each ligand assignment for  $HCO_3^-$  introduced two new parameters for model resolution.

Selecting suitable parameter values was straightforward in practice, since the range of values appropriate for these parameters is largely constrained by the dynamics of  $HCO_3^-$ , which will vary in vivo within the range of 0.05-0.8 mM with 100-1000  $\mu$ bar  $CO_2$ . A value for  $K_{1/2}$  of 0.3 mM placed the midpoint for  $HCO_3^-$  efficacy close to, and marginally above the concentration in the cytosol with an atmospheric  $pCO_2$  of 400  $\mu$ bar. We also examined values of 0.1 and 0.5 mM, thereby biasing the response curve to favor  $HCO_3^-$  efficacy below and above the mean  $HCO_3^-$  concentration, respectively. Values for  $h$  from 1 up to 6 were trialled, subject to a knowledge of the transporter subunit assembly and assuming a maximum

equivalent effectiveness of one binding site per subunit, a feature common among many enzymatic processes<sup>20</sup>. Thus for SLAC, which is thought to assemble functional channels as trimers<sup>21</sup>,  $h$  values of 1, 2 and 3 were trialled. Note that for a  $h$  value of 3, the effective dynamic range (0.05 - 0.95 of fractional activity) is achieved as  $\text{HCO}_3^-$  concentration increases by roughly 5-fold. For example, with a  $K_{1/2}$  of 0.3 mM as the midpoint, the dynamic range for  $\text{HCO}_3^-$  action as a ligand spans the concentration range from 0.12 - 0.7 mM with values below and above giving near-zero and near-maximum activity, respectively.

To identify and rank putative targets for  $\text{HCO}_3^-$  action, we used the results of a global sensitivity analysis of stomatal dynamics based on the OnGuard platform<sup>22</sup>. This study highlighted six core transporters that have the greatest influence on stomatal dynamics, based on the maximum, minimum, and dynamic range of aperture, the opening and closing rates, and the  $[\text{Ca}^{2+}]_i$  oscillation number and frequency. In rank order (highest to lowest), the transporters identified were the endomembrane VCa-ATPase and VCa<sub>in</sub>, the plasma membrane ALMT anion channel and Ca-ATPase, the endomembrane TPK channel, and the plasma membrane H-ATPase. To these, we added a further six transporters, namely the KAT, GORK and SLAC channels at the plasma membrane and the VMAL, VCl, and FV channels at the tonoplast, all of which are known either to be affected by  $\text{CO}_2$  or associated with  $[\text{Ca}^{2+}]_i$ - and ABA-evoked stomatal closure<sup>23,24,25,26</sup>.

Trials introduced  $pC_i$  (dissolved  $\text{CO}_2$ ,  $\text{HCO}_3^-$ ) sensitivities, first to each of these transporters individually, and thereafter to transporters in combination, across the range of parameter values indicated above. Throughout this screening process, we sought the most parsimonious combination of transporters needed to simulate the dynamic range and kinetics of stomatal closure as observed in vivo (see Figure 2). Supplemental Table 2 summarizes the rank scoring arising from the screening and several examples of OnGuard3 outputs are included in Supplemental Figure S1. The most parsimonious solution was the VCa-ATPase+VCa<sub>in</sub> combination. Appendix A3 lists the final set of parameter values as presented in the main text.

**Supplemental Table 2. Analysis of putative pC<sub>i</sub> regulatory targets**

Transporters <sup>a</sup>	Scores <sup>b</sup> :	Dynamic range	Closing rate
VCa-ATPase		4	3
VCa <sub>in</sub> <sup>c</sup>		4	3
VCa <sub>in</sub> <sup>d</sup>		0	0
ALMT		0	0
Ca-ATPase		0	0
TPK		0	0
H-ATPase		0	0
KAT		0	0
GORK		0	0
SLAC		0	0
VMAL		0	0
VCI		0	0
FV		0	0
SLAC+ALMT		0	0
SLAC+ALMT+GORK		0	0
VCa <sub>in</sub> +SLAC+ALMT		0	0
VCa-ATPase+SLAC+ALMT		4	3
VCa-ATPase+VCa <sub>in</sub> <sup>d</sup>		5	5
VCa-ATPase+VCa <sub>in</sub> +SLAC+ALMT		5	5
VCa-ATPase+VCa <sub>in</sub> <sup>d</sup> +GORK		5	5
VCa-ATPase+VCa <sub>in</sub> <sup>d</sup> +SLAC+ALMT+GORK		5	5
VCa-ATPase+VCa <sub>in</sub> <sup>d</sup> +Ca-ATPase		5	5
VCa-ATPase+VCa <sub>in</sub> <sup>d</sup> +H-ATPase		0	0
VCa-ATPase+VCa <sub>in</sub> <sup>d</sup> +TPK		5	5
VCa-ATPase+VCa <sub>in</sub> <sup>d</sup> +FV		5	5
VCa-ATPase+VCa <sub>in</sub> <sup>d</sup> +VCI		5	5
VCa-ATPase+VCa <sub>in</sub> <sup>d</sup> +VMAL		5	5

<sup>a</sup>Knowledge of the basic contributions of each transporter to net solute flux and their association with [Ca<sup>2+</sup>]<sub>i</sub> as a factor in stomatal response to pC<sub>i</sub> removed the need for exhaustive combinatorial trials.

<sup>b</sup>Scale of 0-5 based on efficacy in matching experimental data with pCO<sub>2</sub> steps from 400 to 100 and 1000 μbar (0= no response; units for each 20% increment approaching experimental equivalence).

<sup>c</sup>Ensemble activity, in effect defines the number of available transporters

<sup>d</sup>Inactivation kinetics, defines the rate of activity decline following activation

### Appendix A3. OnGuard3 model parameters for wild-type and *aca* mutant Arabidopsis

OnGuard3 model parameter set RCA5-wt-191120.ogb for wild-type Arabidopsis with *aca* mutant parameter in **bold**. Parameter incorporated in the several tests shown in Supplemental Figure S1 are indicated in *italics*. This file and the corresponding *aca* mutant file are available for download with OnGuard3 from [www.psrp.org.uk](http://www.psrp.org.uk).

Total cell volume = 0.381444 pL; vacuolar volume = 79.1721%

Stomatal Aperture Parameters:

SA:P 'm' = 0.8 atm/ $\mu$ m; SA:P 'n' = 3 atm; SA:V 'R' = 0.05 pL/ $\mu$ m SA:V 'S' = 0.3 pL

Cytosolic Protein Buffering: [Pr] = 0.143584 mM, plso = 6.8, ap = -71

Cytosolic Calcium Buffering: [Bu] = 0.317441 mM, K = 3e-06 M # Ca Sites = 10

Compartmental Solutions (/mM):

	Apoplast	Cytosol	Vacuole
pH	6.5	7.69396	5.26955
K	10	107.737	27.0796
Ca	1	0.0126043	39.8407
Cl	12	16.3431	65.0282
Suc	0.01	0.0390768	0.00466707
MH2	3.23327e-07	2.90048e-07	0.337741
MH	7.93672e-06	0.000111283	0.487677
M	0.00999174	2.18973	36.1144
HCO3	0.0222474	0.347729	0.00130867
CO2	0.0158096	0.0158096	0.0158096

\*\*\* Plasma Membrane Transporters

=====

PM K-in Channel [3000 units] (Inward-Rectifying GHK Channel)

-----

#K' G/Gmax = 9 pOhms  
2-State Voltage Gate:  $V\Omega = -185$  mV,  
Zg = +1.8

Light-Sensitive: NO!

Ligand-Gates:

Ca-inhibited (cytosol): Kd = 3.3e-07, Hill = 4;

H-activated (cytosol): Kd = 6e-08, Hill = 2;

H-activated (apoplast): Kd = 1e-07, Hill = 1;

PM K-out Channel [240 units] (Outward-Rectifying GHK Channel)

-----

#K' G/Gmax = 20 pOhms  
 $V\Omega = +1 \diamond F/RT \diamond \ln([K]_{apo}/10mM)$   
Zg = +2

Light-Sensitive: NO!

Ligand-Gates:

H-inhibited (cytosol): Kd = 3e-08, Hill = 2;

HCO3-activated (cytosol): Kd = 0.0003, Hill = 2;

R-Type Anion Channel [1000 units] (Outward-Rectifying GHK Channel)

-----  
#Cl' G/Gmax = 3.4 pOhms  
#M' G/Gmax = 2 pOhms  
V $\Omega$  = +1  $\diamond$  F/RT  $\diamond$  ln(1e-06mM/[H]cyt)  
Zg = -2

Light-Sensitive: NO!

Ligand-Gates:

Ca-activated (cytosol): Kd= 6e-07, Hill= 4;  
H-activated (cytosol): Kd= 3e-08, Hill= 3;  
HCO3-activated (cytosol): Kd= 0.0003, Hill= 3;

V-Gated Ca-IN [12 units] (Inward-Rectifying GHK Channel)

-----  
#Ca' G/Gmax = 12 pOhms  
V $\Omega$  = +0.5  $\diamond$  F/RT  $\diamond$  ln(2e-09mM/[Ca]cyt)  
Zg = +1

Light-Sensitive: NO!

Ligand-Gates:

Ca-inhibited (cytosol): Kd= 5e-07, Hill= 5;

Anion VIC [300 units] (Outward-Rectifying Ohmic Channel)

-----  
#Cl' G/Gmax = 0.15 pOhms  
#M' G/Gmax = 0.07 pOhms  
Voltage-Independent

Light-Sensitive: NO!

Ligand-Gates:

Ca-activated (cytosol): Kd= 6e-07, Hill= 4;  
H-activated (cytosol): Kd= 4e-08, Hill= 2;  
HCO3-activated (cytosol): Kd= 0.0003, Hill= 1;

H-ATPase [300000 units] (4-State Carrier)

-----  
#H' Stoichiometry = +1; binds at 4->1 (in) and 3->2 (ex);  
K12 = 2000, K23 = 50000, K34 = 500, K41 = 2e+09,  
K21 = 100, K32 = 1e+08, K43 = 10, K14 = 200;

Light-Sensitive: Yes: L $\Omega$  = 50  $\mu$ Einsteins, Fmin = 5%

Ligand-Gates:

Ca-inhibited (cytosol): Kd= 2.5e-07, Hill= 3;

H:Cl Symport [50000 units] (4-State Carrier)

-----  
#H' Stoichiometry = +2; binds at 4->1 (in) and 3->2 (ex);  
#Cl' Stoichiometry = +1; binds at 4->1 (in) and 4->3 (ex);  
K12 = 1000, K23 = 100, K34 = 50000, K41 = 1e+21,  
K21 = 50, K32 = 1e+21, K43 = 100000, K14 = 100;

Light-Sensitive: NO!

Ligand-Gates:

<none>

H:K Symport [16000 units] (4-State Carrier)

-----

#'H' Stoichiometry = +1; binds at 4->1 (in) and 3->2 (ex);  
#'K' Stoichiometry = +1; binds at 4->1 (in) and 4->3 (ex);  
K12 = 2, K23 = 10000, K34 = 100000, K41 = 1e+14,  
K21 = 0.4, K32 = 1e+12, K43 = 1e+10, K14 = 50;

Light-Sensitive: NO!

Ligand-Gates:

<none>

Ca-ATPase [60000 units] (4-State Carrier)

-----

#'Ca' Stoichiometry = +1; binds at 4->1 (in) and 3->2 (ex);  
K12 = 2000, K23 = 10000, K34 = 500, K41 = 1e+15,  
K21 = 2, K32 = 1e+07, K43 = 500, K14 = 1000;

Light-Sensitive: Yes: L $\Omega$  = 50  $\mu$ Einsteins, Fmin = 50%

Ligand-Gates:

Ca-activated (cytosol): Kd= 5e-07, Hill= 2;

HMal symp [40000 units] (Concentration-Driven SYMPORT)

-----

#'H' (Stoichiometry = -3)

#'M' (Stoichiometry = -1)

Fmax = 1e+20

Light-Sensitive: NO!

Ligand-Gates:

<none>

K leak [1 units] (Inward-Rectifying GHK Channel)

-----

#'K' G/Gmax = 1 pOhms  
Voltage-Independent

Light-Sensitive: NO!

Ligand-Gates:

<none>

\*\*\* Tonoplast Transporters

=====

TPK1 [300 units] (Inward-Rectifying Ohmic Channel)

----

#'K' G/Gmax = 90 pOhms  
Voltage-Independent

Light-Sensitive: NO!

Ligand-Gates:

Ca-activated (cytosol): Kd= 3e-06, Hill= 1;

H-activated (cytosol): Kd= 3e-08, Hill= 3;

TPC1 [100 units] (Outward-Rectifying GHK Channel)

----  
#Ca' G/Gmax = 27 pOhms  
#K' G/Gmax = 14 pOhms  
V $\Omega$  = +1  $\diamond$  F/RT  $\diamond$  ln([Ca]<sub>apo</sub>/2mM)  
Z<sub>g</sub> = +2  
Light-Sensitive: NO!  
Ligand-Gates:  
Ca-activated (cytosol): K<sub>d</sub>= 3e-05, Hill= 1;  
H-activated (vacuole): K<sub>d</sub>= 1e-06, Hill= 1;

FV K Channel [800 units] (Inward-Rectifying GHK Channel)

-----  
#K' G/Gmax = 6 pOhms  
2-State Voltage Gate: V $\Omega$  = -30 mV,  
Z<sub>g</sub> = +1  
Light-Sensitive: NO!  
Ligand-Gates:  
Ca-inhibited (cytosol): K<sub>d</sub>= 2e-07, Hill= 1;  
H-inhibited (cytosol): K<sub>d</sub>= 4e-07, Hill= 1;

VCL [300 units] (Inward-Rectifying GHK Channel)

---  
#Cl' G/Gmax = 40 pOhms  
#M' G/Gmax = 10 pOhms  
V $\Omega$  = +1  $\diamond$  F/RT  $\diamond$  ln([H]<sub>apo</sub>/0.005mM)  
Z<sub>g</sub> = -1  
Light-Sensitive: NO!  
Ligand-Gates:  
Ca-activated (cytosol): K<sub>d</sub>= 1e-06, Hill= 1;

VH-ATPase [400000 units] (4-State Carrier)

-----  
#H' Stoichiometry = +2; binds at 4->1 (in) and 3->2 (ex);  
K<sub>12</sub> = 100, K<sub>23</sub> = 1000, K<sub>34</sub> = 0.5, K<sub>41</sub> = 1e+18,  
K<sub>21</sub> = 10, K<sub>32</sub> = 1e+08, K<sub>43</sub> = 5, K<sub>14</sub> = 10000;  
Light-Sensitive: Yes: L $\Omega$  = 50  $\mu$ Einsteins, F<sub>min</sub> = 10%  
Ligand-Gates:  
<none>

VH-PPase [1200000 units] (4-State Carrier)

-----  
#H' Stoichiometry = +1; binds at 4->1 (in) and 3->2 (ex);  
K<sub>12</sub> = 1000, K<sub>23</sub> = 1000, K<sub>34</sub> = 1e+11, K<sub>41</sub> = 3e+09,  
K<sub>21</sub> = 100, K<sub>32</sub> = 5e+09, K<sub>43</sub> = 1e+07, K<sub>14</sub> = 10000;  
Light-Sensitive: Yes: L $\Omega$  = 50  $\mu$ Einsteins, F<sub>min</sub> = 10%  
Ligand-Gates:  
Ca-inhibited (cytosol): K<sub>d</sub>= 1e-07, Hill= 1;  
K-activated (cytosol): K<sub>d</sub>= 0.05, Hill= 1;

VCa-ATPase [800000 units (**320000 units**)] (4-State Carrier)

-----  
#Ca' Stoichiometry = +1; binds at 4->1 (in) and 3->2 (ex);  
K12 = 3000, K23 = 1000, K34 = 1000, K41 = 1e+09,  
K21 = 0.3, K32 = 10000, K43 = 10, K14 = 10000;  
Light-Sensitive: Yes: L $\Omega$  = 50  $\mu$ Einsteins, Fmin = 50%  
Ligand-Gates:  
Ca-activated (cytosol): Kd= 3.5e-07, Hill= 3;  
HCO3-inhibited (cytosol): Kd= 0.0003, Hill= 4;  
Ca-inhibited (vacuole): Kd= 0.04, Hill= 4;

VacCLC [120000 units] (4-State Carrier)

-----  
#H' Stoichiometry = +1; binds at 4->1 (in) and 3->2 (ex);  
#Cl' Stoichiometry = -2; binds at 1->4 (in) and 2->3 (ex);  
K12 = 1000, K23 = 1e+09, K34 = 100, K41 = 1e+10,  
K21 = 1000, K32 = 1e+09, K43 = 10, K14 = 1e+11;  
Light-Sensitive: NO!  
Ligand-Gates:  
H-inhibited (cytosol): Kd= 5e-08, Hill= 2;

VCa [8 units] (Outward-Rectifying GHK Channel)

-----  
#Ca' G/Gmax = 10 pOhms  
V $\Omega$  = +1  $\diamond$  F/RT  $\diamond$  ln(10mM/[Ca]apo)  
+ +0.5  $\diamond$  F/RT  $\diamond$  ln([HCO3]cyt/0.15mM)  
Zg = +4  
Light-Sensitive: NO!  
Ligand-Gates:  
Ca-activated (cytosol): Kd= 5e-07, Hill= 4;  
T-deactivation: switch= [Ca]cyt; Threshold= 0.001mM, T $\Omega$ = 100000ms, reset=  
5%/0.0005mM  
**[X]-dependent t(1/2) ? Yes**  
**X = [HCO3]cyt; activated**  
**K(1/2)= 0.1, Hill= 4**

CAX [100000 units] (Concentration-Driven ANTIPORT)

---  
#H' (Stoichiometry = -3)  
#Ca' (Stoichiometry = +1)  
Fmax = 1e+22  
Light-Sensitive: NO!  
Ligand-Gates:  
Ca-activated (cytosol): Kd= 3e-06, Hill= 1;

ALMT-Mal [600 units] (Inward-Rectifying GHK Channel)

-----  
#M' G/Gmax = 6 pOhms  
2-State Voltage Gate: V $\Omega$  = +0 mV,  
Zg = -2  
Light-Sensitive: NO!  
Ligand-Gates:

H-inhibited (cytosol): Kd= 8.5e-08, Hill= 2;  
Ca-activated (cytosol): Kd= 1e-06, Hill= 1;

NHX [20000 units] (Concentration-Driven ANTIPORT)

---

#'H' (Stoichiometry = -1)

#'K' (Stoichiometry = +1)

Fmax = 100000

Light-Sensitive: NO!

Ligand-Gates:

<none>

METABOLISM

=====

Total Malate (apo/cyt/vac) = 0.01 2.18984 36.9399 mM

Total Sucrose (apo/cyt/vac) = 0.01 0.0390768 0.00466707 mM

Photosynthesis:

Suc s-max = 10 fmol/h, L $\Omega$  = 50  $\mu$ E

Mal s-max = 0 fmol/h, L $\Omega$  = 50  $\mu$ E

Catabolism: R-max = 10 fmol/h, K $\Omega$  = 1 mM

Suc <-> Mal Conversion:

R-max = 5 fmol/h, K $\Omega$ (S) = 0.1 mM, K $\Omega$ (M) = 10 mM

Mid-point pH = 7.7, pH gradient = +64

Red Light Cycle: Dawn= 00:00, Noon= 04:00, Dusk= 16:00; L-Max= 1100  $\mu$ E, Pattern= 'Bell'

Blue Light Cycle: Dawn= 00:00, Noon= 02:00, Dusk= 12:00; L-Max= 1100  $\mu$ E, Pattern= 'Bell'

WUE ...

=====

Leaf Geometry: F(s) = 100 /mm $\leq$ ; Stomatal Length = 8  $\mu$ m, Depth = 15  $\mu$ m.

Subepidermal Depth = 300  $\mu$ m, Space Fraction = 50 %.

Relative Water Feed factor = 40

AQUAPORINS ...

=====

Population = Default Aquaporins (100 %)

Flux Restriction Factor = 0.004

Ligand: Ca (inhibited); Kd = 4.5e-07, Hill Coefficient = 6.

CRR

=====

CRR accelerator YES

Solute K

Capacity fmol = 14

Second Capacity fmol = 0.5  
Max Recovery rate fmol/s = 0.006  
Rate order = 1  
Turgor sensitivity YES  
Midpint atm = 7  
Sigmoid /atm = 2

TEMPERATURE ...  
=====

Leaf Temperature = 25 C, Air Temperature = 25 C  
Metabolic Temperature Coefficient (Q10) = 2

Current 'time' in model = 00:00:00.00; RH = 70

=====

## Citations

- 1 von Caemmerer, S. Steady-state models of photosynthesis. *Plant Cell and Environment* **36**, 1617-1630, doi:10.1111/pce.12098 (2013).
- 2 Evans, J. R., Sharkey, T. D., Berry, J. A. & Farquhar, G. D. CARBON ISOTOPE DISCRIMINATION MEASURED CONCURRENTLY WITH GAS-EXCHANGE TO INVESTIGATE CO<sub>2</sub> DIFFUSION IN LEAVES OF HIGHER-PLANTS. *Australian Journal of Plant Physiology* **13**, 281-292, doi:10.1071/pp9860281 (1986).
- 3 Farquhar, G. D. & Sharkey, T. D. STOMATAL CONDUCTANCE AND PHOTOSYNTHESIS. *Annual Review of Plant Physiology and Plant Molecular Biology* **33**, 317-345, doi:10.1146/annurev.pp.33.060182.001533 (1982).
- 4 Morison, J. I. L., Lawson, T. & Cornic, G. Lateral CO<sub>2</sub> diffusion inside dicotyledonous leaves can be substantial: Quantification in different light intensities. *Plant Physiology* **145**, 680-690 (2007).
- 5 Morison, J. I. L. *et al.* Lateral diffusion of CO<sub>2</sub> in leaves is not sufficient to support photosynthesis. *Plant Physiology* **139**, 254-266 (2005).
- 6 Parkhurst, D. F., Wong, S. C., Farquhar, G. D. & Cowan, I. R. GRADIENTS OF INTERCELLULAR CO<sub>2</sub> LEVELS ACROSS THE LEAF MESOPHYLL. *Plant Physiology* **86**, 1032-1037, doi:10.1104/pp.86.4.1032 (1988).
- 7 Von Caemmerer, S. & Farquhar, G. D. Some relationships between the biochemistry of photosynthesis and the gas exchange of leaves. *Planta* **153**, 376-387 (1981).
- 8 Ogren, E. & Evans, J. R. PHOTOSYNTHETIC LIGHT-RESPONSE CURVES .1. THE INFLUENCE OF CO<sub>2</sub> PARTIAL-PRESSURE AND LEAF INVERSION. *Planta* **189**, 182-190, doi:10.1007/bf00195075 (1993).
- 9 Lindskog, S. Structure and mechanism of carbonic anhydrase. *Pharmacology & Therapeutics* **74**, 1-20, doi:10.1016/s0163-7258(96)00198-2 (1997).
- 10 Lindskog, S. *et al.* KINETICS AND MECHANISM OF CARBONIC-ANHYDRASE ISOENZYMES. *Annals of the New York Academy of Sciences* **429**, 61-75, doi:10.1111/j.1749-6632.1984.tb12315.x (1984).
- 11 Wang, Y. *et al.* Unexpected Connections between Humidity and Ion Transport Discovered using a Model to Bridge Guard Cell-to-Leaf Scales. *Plant Cell* **29**, 2921-2139, doi:10.1105/tpc.17.00694 (2017).
- 12 Garcia-Mata, C. *et al.* Nitric oxide regulates K<sup>+</sup> and Cl<sup>-</sup> channels in guard cells through a subset of abscisic acid-evoked signaling pathways. *Proceedings Of The National Academy Of Sciences Of The United States Of America* **100**, 11116-11121 (2003).
- 13 Grabov, A. & Blatt, M. R. A steep dependence of inward-rectifying potassium channels on cytosolic free calcium concentration increase evoked by hyperpolarization in guard cells. *Plant Physiology* **119**, 277-287 (1999).
- 14 Grabov, A. & Blatt, M. R. Membrane voltage initiates Ca<sup>2+</sup> waves and potentiates Ca<sup>2+</sup> increases with abscisic acid in stomatal guard cells. *Proceedings Of The National Academy Of Sciences Of The United States Of America* **95**, 4778-4783 (1998).
- 15 Lemtiri-Chlieh, F. *et al.* Inositol hexakisphosphate mobilizes an endomembrane store of calcium in guard cells. *Proceedings Of The National Academy Of Sciences Of The United States Of America* **100**, 10091-10095 (2003).
- 16 Gilroy, S., Fricker, M. D., Read, N. D. & Trewavas, A. J. Role of calcium in signal transduction of *Commelina* guard cells. *Plant Cell* **3**, 333-344 (1991).
- 17 Minguet-Parramona, C. *et al.* An Optimal Frequency in Ca<sup>2+</sup> Oscillations for Stomatal Closure Is an Emergent Property of Ion Transport in Guard Cells. *Plant Physiology* **170**, 32-45, doi:10.1104/pp.15.01607 (2016).
- 18 Chen, Z. H. *et al.* Systems Dynamic Modeling of the Stomatal Guard Cell Predicts Emergent Behaviors in Transport, Signaling, and Volume Control. *Plant Physiology* **159**, 1235-1251 (2012).
- 19 Hills, A., Chen, Z. H., Amtmann, A., Blatt, M. R. & Lew, V. L. OnGuard, a Computational Platform for Quantitative Kinetic Modeling of Guard Cell Physiology. *Plant Physiology* **159**, 1026-1042 (2012).

- 20 Segel, I. H. *Enzyme Kinetics*. (Wiley Interscience, 1993).
- 21 Chen, Y.-h. *et al.* Homologue structure of the SLAC1 anion channel for closing stomata in leaves. *Nature* **467**, 1074-U1157, doi:10.1038/nature09487 (2010).
- 22 Violet-Chabrand, S. *et al.* Global Sensitivity Analysis of OnGuard Models Identifies Key Hubs for Transport Interaction in Stomatal Dynamics. *Plant Physiology* **174**, 680-688, doi:10.1104/pp.17.00170 (2017).
- 23 Jezek, M. & Blatt, M. R. The Membrane Transport System of the Guard Cell and Its Integration for Stomatal Dynamics. *Plant Physiology* **174**, 487-519, doi:10.1104/pp.16.01949 (2017).
- 24 Roelfsema, M. R. G. & Hedrich, R. In the light of stomatal opening: new insights into 'the Watergate'. *New Phytologist* **167**, 665-691 (2005).
- 25 Kollist, H., Nuhkat, M. & Roelfsema, M. R. G. Closing gaps: linking elements that control stomatal movement. *New Phytologist* **203**, 44-62, doi:10.1111/nph.12832 (2014).
- 26 Webb, A. A. R., McAinsh, M. R., Mansfield, T. A. & Hetherington, A. M. Carbon dioxide induces increases in guard cell cytosolic free calcium. *Plant Journal* **9**, 297-304 (1996).

## Supplemental Figures

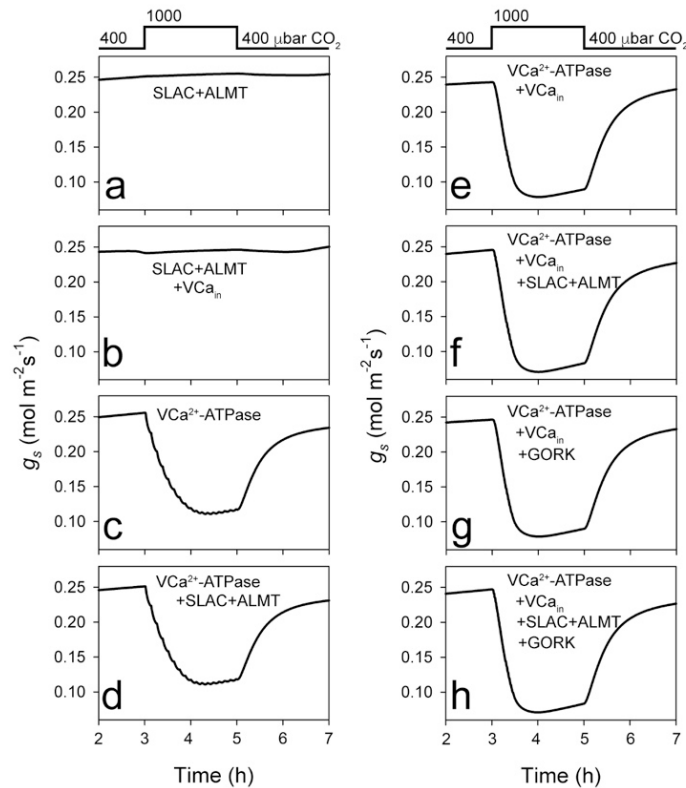


### Figure S1. OnGuard3 reveals a critical dependence on endomembrane $\text{Ca}^{2+}$ release and resequestration to drive stomatal closure with $\text{CO}_2$ .

Shown are outputs for stomatal conductance ( $g_s$ ) with 2-h steps from 400 to 1000  $\mu\text{bar CO}_2$  using the OnGuard3 model parameters in Appendix 3 with  $p\text{C}_i$  ( $\text{HCO}_3^-$ ,  $\text{CO}_2$ ) dependencies assigned, as indicated. Assignment are (a) to enhance the SLAC and ALMT anion channels, and (b) additionally to accelerate inactivation gating of the endomembrane  $\text{VCa}_{\text{in}}$   $\text{Ca}^{2+}$  channels; (c) to suppress endomembrane  $\text{VCa}^{2+}$ -ATPase activity, and (d) additionally to enhance the SLAC and ALMT anion channels; (e) to suppress endomembrane  $\text{VCa}^{2+}$ -ATPase activity and accelerate inactivation gating of the endomembrane  $\text{VCa}_{\text{in}}$   $\text{Ca}^{2+}$  channels, and (f) additionally to enhance SLAC and ALMT anion channels, or additionally (g) to enhance GORK  $\text{K}^+$  channels, or (h) additionally to enhance SLAC, ALMT and GORK  $\text{K}^+$  channels. Parameter settings for the transporters individually and in combination are the same as those listed in Appendix 3 with  $p\text{C}_i$  assignments listed in *italics*. A summary of the pathway to resolving the primary actions for  $p\text{C}_i$  is set out in Supplemental Appendix A2.

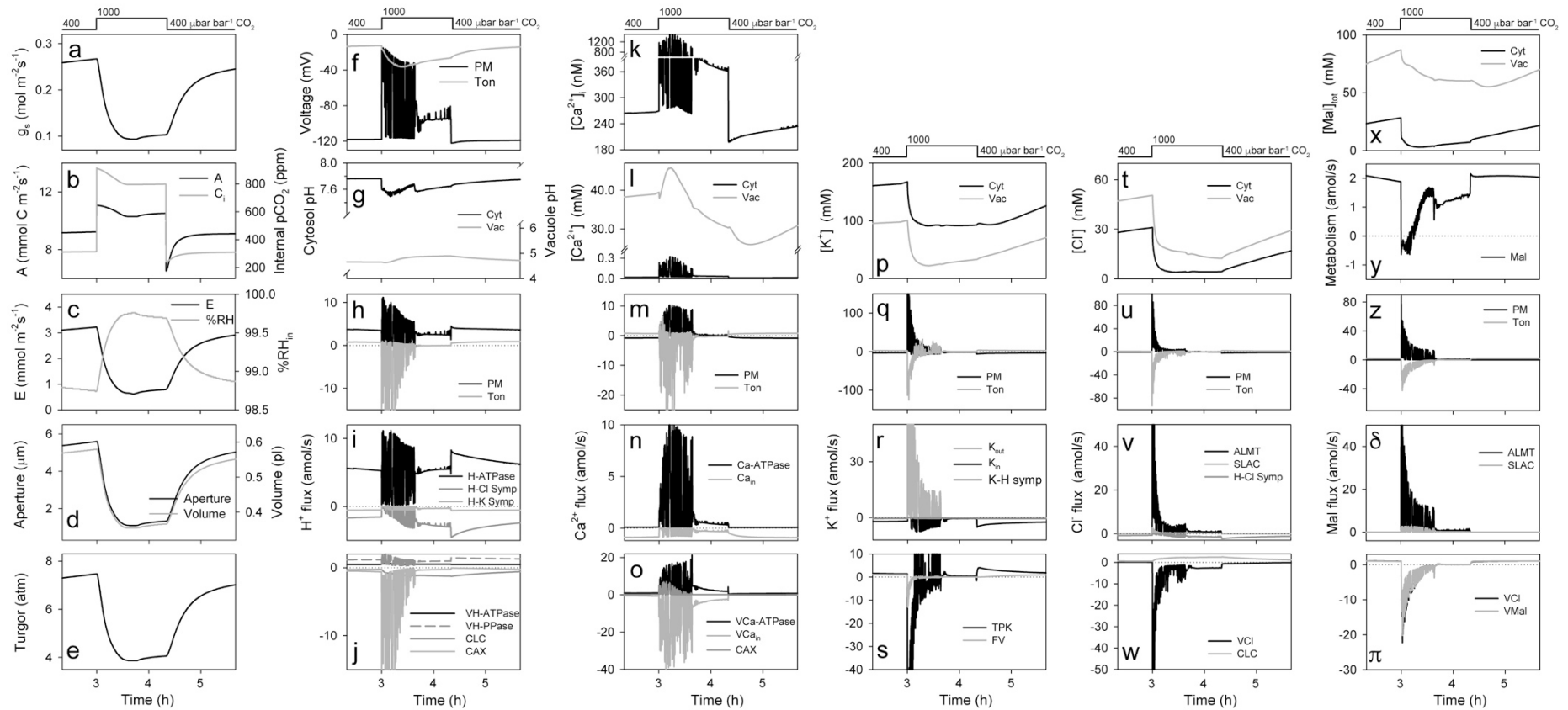


**Figure S2. OnGuard3 outputs for guard cell pH,  $\text{Ca}^{2+}$ , osmotic solute transport and Mal synthesis of the wild type.**

Outputs generated using a standard light:dark cycle as described previously<sup>1</sup>. Model parameters are listed in Appendix 2. Graphs are separated in columns for outputs pertaining aperture and gas exchange (a-e), to  $\text{H}^+$  (f-j),  $\text{Ca}^{2+}$  (k-o),  $\text{K}^+$  (p-s),  $\text{Cl}^-$  (t-w), and Mal (x- $\pi$ ). A 90-min step from 400 to 1000  $\mu\text{bar}$   $\text{CO}_2$  was introduced 3 h into the light period as indicated above each graph column. Corresponding macroscopic, osmotic solute, and  $\text{K}^+$  current outputs are shown also in Figures 3 and 4. Note that positive flux is defined as movement of the ionic species (not charge) out of the cytosol, either across the plasma membrane or the tonoplast. Oscillations in a number of fluxes are a consequence of the corresponding oscillations in voltage and cytosolic free  $[\text{Ca}^{2+}]_i$  ( $[\text{Ca}^{2+}]_i$ ) (see Figure 3a-c).

(a-e) Phenomenological outputs of stomatal conductance ( $g_s$ ; a), carbon assimilation rate ( $A$ ; b), transpiration rate ( $E$ ) and percent relative humidity (%RH) at  $p$  inside the leaf (c), stomatal aperture and guard cell volume (d), and guard cell turgor pressure (e).

(f-j) Plasma membrane and tonoplast voltages (f), Cytosolic and vacuolar pH (g), net  $H^+$  flux across the plasma membrane and tonoplast (h), and  $H^+$  flux through each of the relevant transporters at the plasma membrane (i) and tonoplast (j).

(k-o) Cytosolic-free  $[Ca^{2+}]$  ( $[Ca^{2+}]_i$ , k), total cytosolic and vacuolar  $[Ca^{2+}]$  (l), net  $Ca^{2+}$  flux across the plasma membrane and tonoplast (m), and  $Ca^{2+}$  flux through each of the relevant transporters at the plasma membrane (n) and tonoplast (o).

(p-s) Total cytosolic and vacuolar  $[K^+]$  (p), net  $K^+$  flux across the plasma membrane and tonoplast (q), and  $K^+$  flux through each of the relevant transporters at the plasma membrane (r) and tonoplast (s).

(t-w) Total cytosolic and vacuolar  $[Cl^-]$  (t), net  $Cl^-$  flux across the plasma membrane and tonoplast (u), and  $Cl^-$  flux through each of the relevant transporters at the plasma membrane (v) and tonoplast (w).

( $x-\pi$ ) Total cytosolic and vacuolar  $[Mal]$  (x), Mal synthesis (y), net Mal flux across the plasma membrane and tonoplast (z), and Mal flux through each of the relevant transporters at the plasma membrane ( $\delta$ ) and tonoplast ( $\pi$ ). Note in (y), positive values indicate Mal synthesis, negative indicate Mal consumption.

In each case, relaxations are the consequence of the intrinsic interactions that arise from the properties of each transporter, of Mal metabolism, and of photosynthetic consumption of  $CO_2$ . Counterintuitively,  $pC_i$  (Figure 2A) promotes an elevation in  $[Ca^{2+}]_i$  initially suppressing the  $VCa^{2+}$ -ATPase and accelerating  $VCa_{in}$  gating before the elevated  $[Ca^{2+}]_i$  enhances  $VCa^{2+}$ -ATPase activity to re-sequester  $Ca^{2+}$  from the cytosol, there by initiating interactive oscillations between  $[Ca^{2+}]_i$  and plasma membrane voltage. The oscillations in plasma membrane voltage are driven by antiparallel changes in flux through the SLAC, ALMT (v,  $\delta$ ), GORK ( $K_{out}$ , r) and KAT ( $K_{in}$ , r) channels. SLAC, ALMT and KAT activities, as well as flux through the  $H^+$ -ATPase, are coupled to  $[Ca^{2+}]_i$ . These oscillations also impact on  $[Ca^{2+}]_i$ -sensitive transport at the tonoplast, notably the TPK and FV  $K^+$  channels and the VCl and VMal anion channels, in effect flushing  $K^+$ ,  $Cl^-$  and Mal from the vacuole through the cytosol and across the plasma membrane to the apoplast.

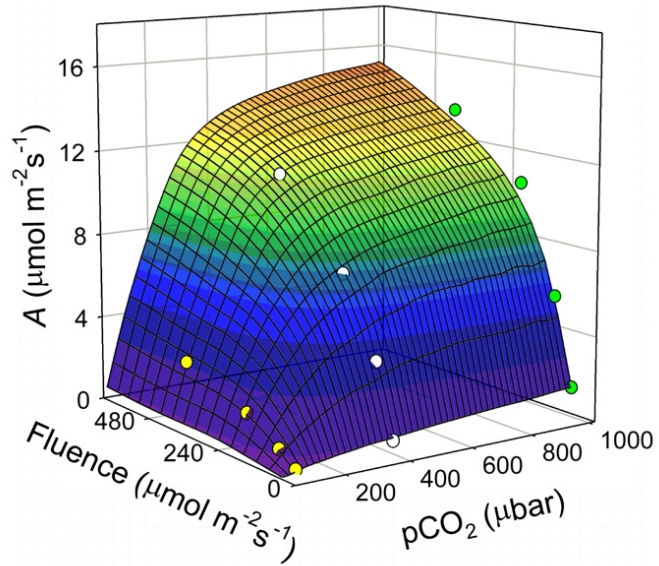
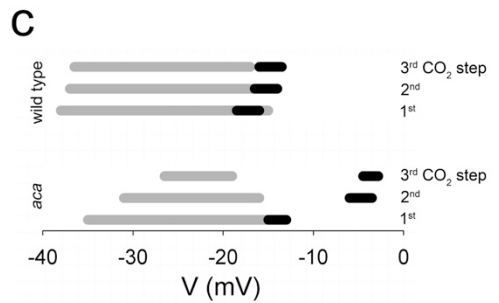
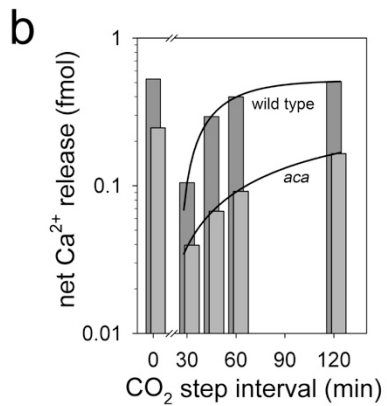
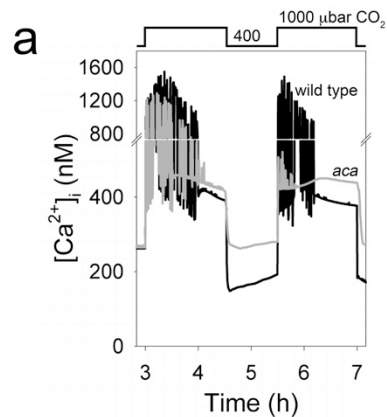


Figure S3. **Steady-state of carbon assimilation rate ( $A$ ) and its dependence on  $\text{pCO}_2$  and PAR fluence rate.**

Surface plot was determined from the OnGuard3 model and is overlaid with experimental measurements (symbols: green, white, yellow for 1000, 400 and 100  $\mu\text{bar}$   $\text{CO}_2$ , respectively) from Arabidopsis. The corresponding experimental and modelled values for stomatal conductance are shown in Figure 2. Model parameters are summarised in Appendix 3.



**Figure S4. Reducing endomembrane  $\text{Ca}^{2+}$ -ATPase activity in OnGuard3 suppresses cytosolic-free  $[\text{Ca}^{2+}]_i$  ( $[\text{Ca}^{2+}]_i$ ) oscillations and mean  $[\text{Ca}^{2+}]_i$ , and enhances the latency in net endomembrane  $\text{Ca}^{2+}$  release.**

OnGuard3 model parameters for the wild type (Appendix 2) were modified to simulate the *aca* mutants, as in Figure 5D, by reducing the membrane density of  $\text{VCa}^{2+}$ -ATPases from 800,000 to 320,000, consistent with a 60% decline in capacity. Qualitatively similar results were obtained on reducing the density of  $\text{VCa}^{2+}$ -ATPases by 50-80%.

(a) OnGuard3 model outputs for  $[\text{Ca}^{2+}]_i$  corresponding to wild-type (black) and *aca* mutant (grey) Arabidopsis challenged with successive 90-min steps from 400 to 1000  $\mu\text{bar}$   $\text{CO}_2$  (*above*). Note the reduced amplitude in  $[\text{Ca}^{2+}]_i$  oscillations in the *aca* mutant, especially on the second  $\text{pCO}_2$  step and the loss in undershoot of  $[\text{Ca}^{2+}]_i$  on return to 400  $\mu\text{bar}$   $\text{pCO}_2$ .

(b) Net endomembrane  $\text{Ca}^{2+}$  release during 90-min steps to 1000  $\mu\text{bar}$   $\text{pCO}_2$  as in (A) with intervening periods at 400  $\mu\text{bar}$   $\text{pCO}_2$  for periods of 30, 45, 60 and 120 min. Values are for wild-type (dark grey) and *aca* mutant (light grey) Arabidopsis. Least-squares fitting<sup>2</sup> to single exponential functions (solid lines) indicated latencies in recovery of net  $\text{Ca}^{2+}$  flux with half-times of  $16 \pm 1$  and  $52 \pm 3$  min for the wild type and *aca* mutant, respectively.

(c) The midpoint voltage for gating of the  $\text{VCa}_{\text{in}}$   $\text{Ca}^{2+}$  channel necessarily incorporates a sensitivity to vacuolar  $[\text{Ca}^{2+}]$  that, like many known endomembrane  $\text{Ca}^{2+}$  channels, self-limits channel activity. For the guard cells, this sensitivity ensures the channel does not fully deplete endomembrane stores during stomatal closure<sup>3,4</sup>. In simulation, the consequence of successive challenges with 1000  $\mu\text{bar}$   $\text{pCO}_2$  is to displace this gating midpoint voltage range (black bars) by more than +15 mV from the free-running tonoplast voltage (grey bars), suppressing subsequent  $\text{Ca}^{2+}$  release and reducing endomembrane  $\text{Ca}^{2+}$  flux (b) and  $[\text{Ca}^{2+}]_i$  elevations (a), and thereby slowing stomatal kinetics in successive exposures to elevated  $\text{pCO}_2$  (Figure 5).

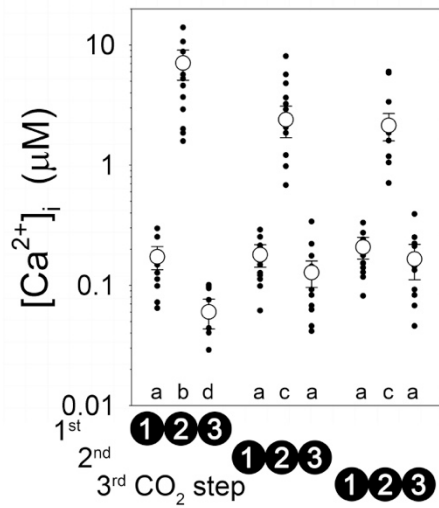


**Figure S5. Reducing the interval between 100  $\mu bar$   $pCO_2$  steps suppresses cytosolic-free  $[Ca^{2+}]_i$  elevations.**

Cytosolic-free  $[Ca^{2+}]_i$  recorded from Arabidopsis guard cells pre-loaded with the  $Ca^{2+}$ -sensitive fluorescent dye Fura-Red and challenged with 1000  $\mu bar$   $CO_2$  as in Figure 4e-g with stomata from the same epidermal peel challenged with  $pCO_2$  steps separated by 30-min intervals. Analysis of the endpoints for  $[Ca^{2+}]_i$  recorded from  $n=12$  independent experiments shows a highly significant rise in  $[Ca^{2+}]_i$  with  $pCO_2$  elevation and undershoot on its recovery in on first challenge with 1000  $\mu bar$   $CO_2$ . With subsequent  $pCO_2$  steps, the maximum rise was significantly reduced and the undershoot was suppressed. Time points are cross-referenced to the experimental protocol in Figure 4f by the circled numbers. Filled symbols are individual experimental data with means  $\pm$ SE indicated by the open symbols and error bars. Letters indicate significant differences ( $P < 0.02$ ).

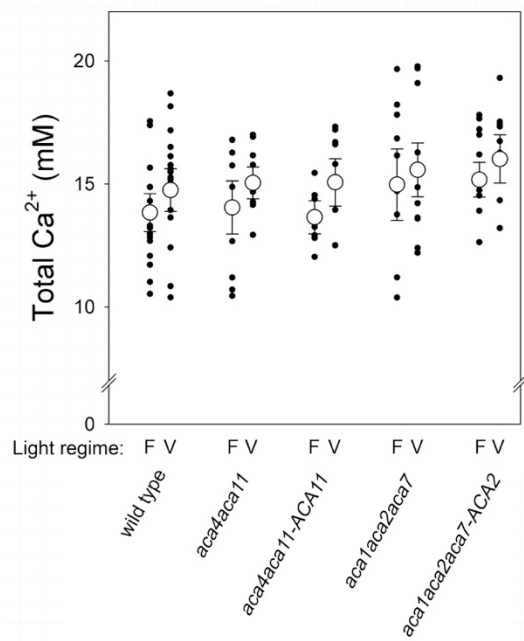


**Figure S6. Total foliar Ca<sup>2+</sup> content is unaffected by mutation of endomembrane ACA Ca<sup>2+</sup>-ATPases.**

Wild-type, mutant and complemented Arabidopsis lines grown under cycles of 9 h:15 h L:D and were given the same total diel fluence with daylight regimes of fixed (F) and variable (V) light as indicated (see Methods). Total foliar Ca<sup>2+</sup> was determined from dried and extracted aerial biomass and concentrations calculated from the corresponding fresh weight assuming a 1:1 w/v ratio. Data points are for individual plants and open symbols indicate the means  $\pm$ SE [n= 20 (wild type) and 10 (mutant and complemented lines)]. No significant difference was found at P<0.05.

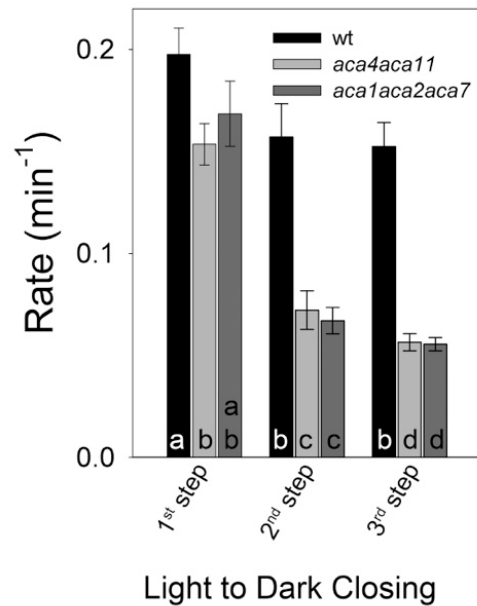


**Figure S7. Latency in  $g_s$  relaxation with light is strongly affected in mutants lacking endomembrane  $\text{Ca}^{2+}$ -ATPases.**

Wild-type (black bars), *aca4aca11* (light grey) and *aca1aca2aca7* (dark grey) mutant plants were challenged under constant 400  $\mu\text{bar}$   $\text{CO}_2$  with three successive cycles from 200 to 0  $\mu\text{mol m}^{-2}\text{s}^{-1}$  photosynthetically active radiation (PAR) separated by 45-min intervals at 200  $\mu\text{mol m}^{-2}\text{s}^{-1}$  PAR, as indicated. Data in each case are from  $n \geq 6$  independent experiments as in Figure 5. Letters indicate significant differences ( $P < 0.02$ ). Note the substantial slowing in  $g_s$  kinetics of the mutant in the second and third steps to 0  $\mu\text{mol m}^{-2}\text{s}^{-1}$  PAR.

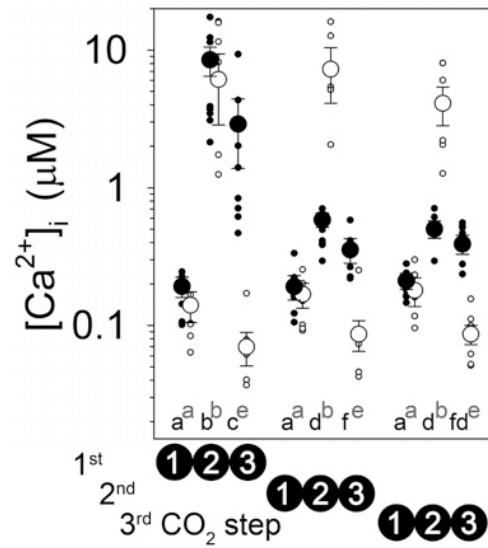


**Figure S8. Repeated challenges with high partial pressure of  $CO_2$  ( $pCO_2$ ) transitions uncover a latency in the recovery of  $[Ca^{2+}]_i$  elevations.**

Cytosolic-free  $[Ca^{2+}]_i$  recorded from *aca1aca2aca7* mutant and *ACA2*-complemented *aca1aca2aca7* mutant guard cells pre-loaded with the  $Ca^{2+}$ -sensitive fluorescent dye Fura-Red and challenged with 1000  $\mu bar$   $CO_2$ . Data are means  $\pm$ SE of  $n \geq 9$  independent experiments as in Figure 5. Note the suppression in elevated  $[Ca^{2+}]_i$  with successive  $pCO_2$  cycles. Time points are cross-referenced to the experimental protocol (Figure 5e) by the circled numbers. Small circles are individual experimental data with means  $\pm$ SE indicated by large circles and error bars. Filled and open symbols are *aca1aca2aca7* mutant and *ACA2*-complemented *aca1aca2aca7* mutant guard cells, respectively. Letters indicate significant differences ( $P < 0.02$ ).

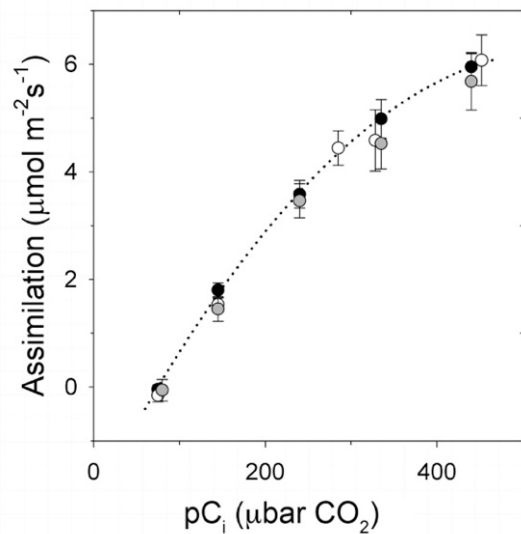


**Figure S9. Erosion in the biomass of Ca<sup>2+</sup>-ATPase mutant Arabidopsis is not related to a reduction in photosynthetic capacity.**

Plants of the *aca4aca11* (open circles) and *aca1aca2aca7* (grey circles) mutants showed CO<sub>2</sub> assimilation rates under saturating photosynthetically-active radiation (PAR, 600 µmol m<sup>-2</sup> s<sup>-1</sup>) that was statistically indistinguishable from wild-type plants (black circles) across the physiological range of internal CO<sub>2</sub> concentrations.

#### Citations

- 1 Wang, Y. *et al.* Unexpected Connections between Humidity and Ion Transport Discovered using a Model to Bridge Guard Cell-to-Leaf Scales. *Plant Cell* **29**, 2921-2139 (2017).
- 2 Marquardt, D. An algorithm for least-squares estimation of nonlinear parameters. *J. Soc. Ind. Appl. Math.* **11**, 431-441 (1963).
- 3 Hills, A., Chen, Z. H., Amtmann, A., Blatt, M. R. & Lew, V. L. OnGuard, a Computational Platform for Quantitative Kinetic Modeling of Guard Cell Physiology. *Plant Physiology* **159**, 1026-1042 (2012).
- 4 Chen, Z. H. *et al.* Systems Dynamic Modeling of the Stomatal Guard Cell Predicts Emergent Behaviors in Transport, Signaling, and Volume Control. *Plant Physiology* **159**, 1235-1251 (2012).